JCTC Journal of Chemical Theory and Computation

Article

pubs.acs.org/JCTC

A Polarizable and Transferable PHAST CO_2 Potential for Materials Simulation

Ashley L. Mullen, Tony Pham, Katherine A. Forrest, Christian R. Cioce, Keith McLaughlin, and Brian Space*

Department of Chemistry, University of South Florida, 4202 East Fowler Avenue, CHE 205, Tampa, Florida 33620-5250, United States

ABSTRACT: Reliable PHAST (Potentials with High Accuracy Speed and Transferability) intermolecular potential energy functions for CO_2 have been developed from first principles for use in heterogeneous systems, including one with explicit polarization. The intermolecular potentials have been expressed in a transferable form and parametrized from nearly exact electronic structure calculations. Models with and without explicit many-body polarization effects, known to be important in simulation of interfacial processes, are constructed. The models have been validated on pressure−density isotherms of bulk CO_2 and adsorption in three metal−organic framework (MOF) materials. The present models appear to offer advantages over high quality fluid/liquid state potentials in describing CO_2 interactions in interfacial environments where sorbates adopt orientations not commonly explored in bulk fluids. Thus, the nonpolar CO_2-PHAST and polarizable CO_2-PHAST* potentials are recommended for materials/interfacial simulations.

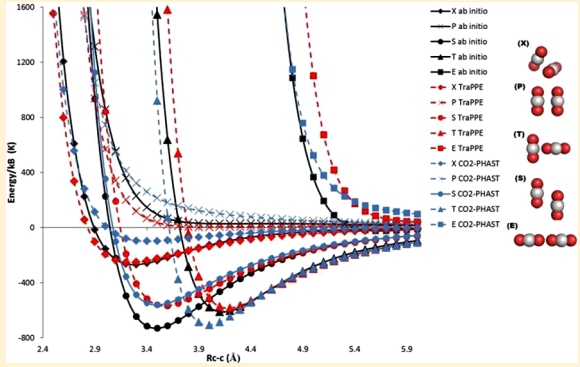

I. INTRODUCTION

Carbon dioxide capture and sequestration are important endeavors to help with the growing climate change. Existing carbon dioxide capture methods include extraction with an aqueous amine solution, separation and capture with membranes, and adsorption within activated charcoal, zeolites, and metal−organic framework (MOF) materials.[1,2] To expedite the design and testing of new materials for such applications, many chemists are using computational methods such as molecular dynamics and Monte Carlo simulations to model gas adsorption and separation.[2−5] It would also be desirable to model carbon dioxide under geological conditions associated with sequestration.[6] Existing potential energy surfaces to molecularly model CO_2 are parametrized for neat simulation and may not accurately capture highly anisotropic and complex many-body interactions. Thus, a transferable and accurate carbon dioxide potential that includes anisotropy and polarization is desirable for modeling adsorption in heterogeneous and dense systems. The potential energy form is chosen to capture intermolecular interactions with a minimum of terms that reflect the essential physical interactions to maintain transferability of the surface.

Intermolecular potentials can be constructed from (1) fitting to experimental data such as solid CO_2 lattice parameters and lattice energies,[7−9] second virial coefficients,[8] liquid densities, and vapor−liquid equilibria,[10−15] (2) fitting to *ab initio* calculations,[16−22] or some combination of the two.[23,24] The limitations of method 1 are that experimental measurements can cover only a limited region of the potential energy surface represented in the fluid and limited information about the anisotropy of the potential is given. Scheme 2, made sufficiently accurate by advances in electronic structure methods and computer hardware,[25] can provide information for a wide range of separation distances and many dimer configurations, both of which lead to a fuller understanding of the potential energy surface. Reasonably simple pair potentials of type 1, especially those with Lennard-Jones functions representing van der Waals interactions, have the capability of being used in simulations of heterogeneous media because of mixing rule conventions. High quality intermolecular potentials of type 2 are often chosen as complex functional forms. They produce high fidelity analytic representations, which require many parameters and are thus limited to model only pure carbon dioxide. Here, we produce a potential of type 2 that is fit to a transferable form that includes explicit induction to capture essential many-body effects, although methods exist to include many-body dispersion as well.[26] The resulting potential form is a compromise in that it cannot exactly reproduce the *ab initio* dimer potentials for carbon dioxide because of the limited, compact description. However, it does a reasonable job for all geometries (including those important in sorption but not in bulk fluids) and includes polarization, thus making the potential suitable for simulations with strong interactions. Therefore, the resulting potential, while effective for bulk simulations, is also efficacious in

Received: June 27, 2013
Published: November 13, 2013

modeling CO_2 in heterogeneous environments and at extreme conditions.

II. METHODS

A. Quantum Mechanical Calculations. The carbon dioxide molecule was approximated as linear and rigid with a C−O bond length of 1.162 Å as determined by rotational spectra;[27] adding flexibility to the model is little additional effort.[28] Five distinct orientations (Figure 1) were chosen as a

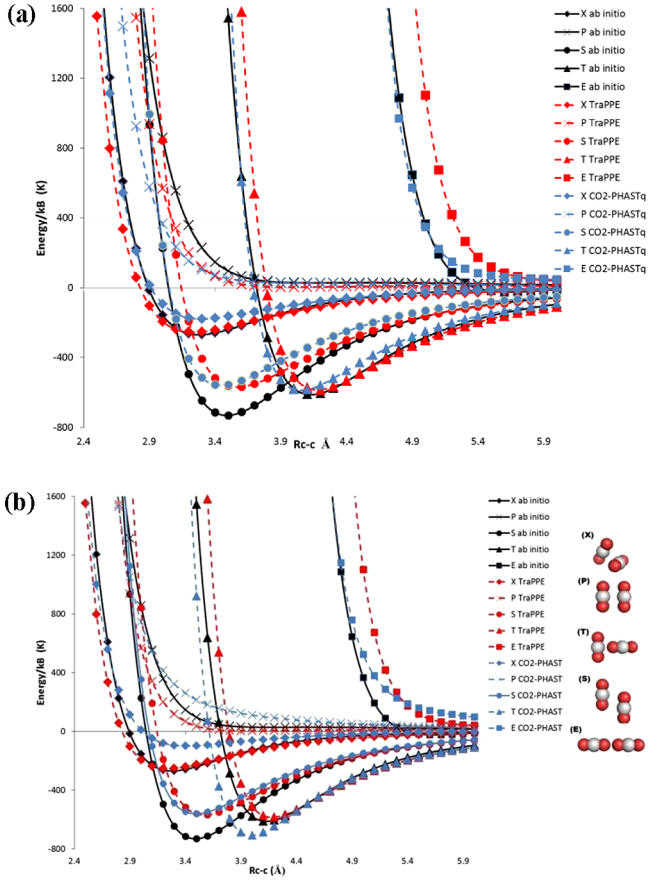

Figure 1. *Ab initio* curves and potential energy curves of carbon dioxide dimers comparing (a) TraPPE and CO_2-PHASTq to *ab initio* and (b) TraPPE and CO_2-PHAST to *ab initio*. Note that the polarizable PHASTq* and PHAST* curves are visually identical to the nonpolar PHASTq and PHAST curves, respectively, shown here.

subspace of the complete CO_2−CO_2 Born−Oppenheimer surface, and the interaction energy was calculated over the domain of center-of-mass separation for the monomers from 2.5 to 8.0 Å in 0.1 Å increments.[21,29] All *ab initio* calculations were performed using Molpro[25] at the CCSD(T)[30] level of theory, with basis functions of Dunning et al. (aug-cc-PVTZ/QZ).[31,32] The total energy was extrapolated to the complete basis set limit,[33] and basis set superposition error was corrected by the counterpoise method.[34]

The *ab initio* quadrupole tensor was calculated at the CCSD(T)/aug-cc-pV5Z level of theory via the finite-field method with a homogeneous field strength of 0.005 e^{-1} a_0^{-1} E_h.[35] For a linear molecule, the permanent molecular electric quadrupole moment is $\Theta \equiv \Theta_{zz} = -2\Theta_{yy} = -2\Theta_{xx}$ and was found to be $\Theta = -4.284$ DÅ for CO_2, a value comparable to experimental and electronic structure results.[36−38] Note that some potentials use an older experimental estimate that is slightly off, and most efficacious potentials do not reproduce the true monomer quadrupole.[11]

The molecular polarizability tensor of carbon dioxide was computed at the time-dependent Hartree−Fock[39] TDHF/aug-cc-pVQZ level of theory. The tensor values were rescaled so that the isotropic polarizability matched the experimental result of 2.507 Å^3 and kept the ratio of *XX* to *ZZ* fixed. Values for the *ab initio* polarizability tensor and the rescaled tensor are given in Table 1.

Table 1. CO_2 Molecular Polarizability Tensor Calculated via Time-Dependent Hartree−Fock along with Its Rescaled Components[a]

component	TDHF, Å^3	rescaled, Å^3
XX	1.7727	1.8885
YY	1.7727	1.8885
ZZ	3.5146	3.7441
isotropic	2.3533	2.507

[a]The components were rescaled such that the isotropic polarizability matched experiment with the constraint that the ratio of *ab initio* values *XX*/*ZZ* be preserved.

B. Many-Body Polarization. The interest of this work is to develop an intermolecular potential energy function effective in charged and polar heterogeneous environments. Such a model requires inclusion of induction effects that are essentially many-body; the Thole−Applequist atomic point polarizability model was adopted to capture these interactions. A brief description of the polarization model as applied here is presented, and a more thorough description can be found elsewhere.[29,40,41] For any atom, the atomic point dipole is

$$\mu_i^m = \alpha_i(E_i^m + E_i'^m) \tag{1}$$

$$\mu_i^m = \alpha_i(E_i^m - \sum_{j,n} T_{ij}^{mn}\mu_j^n) \tag{2}$$

where α_i is the atomic site polarizability, E^m is the static contribution, and E'^m is the induced contribution to the electrostatic field vector. The induced contribution can be written in terms of the dipole field tensor, T_{ij}, which can be constructed from the positions and scalar point polarizabilities of the system.

$$T_{ii}^{mn} = 0 \tag{3}$$

$$T_{ij}^{mn} = \frac{\delta_{mn}}{r_{ij}^3} - \frac{3r_{ij}^m r_{ij}^n}{r_{ij}^5} \tag{4}$$

However, eq 4 needs to be corrected for nonphysical results at small distances. The exponential damping function given in eq 5 was utilized.[41]

$$T_{ij}^{mn} = \frac{\delta_{mn}}{r_{ij}^3}\left(1 - \left(\frac{\lambda^2 r_{ij}^2}{2} + \lambda r_{ij} + 1\right)e^{-\lambda r_{ij}}\right) - \frac{3r_{ij}^m r_{ij}^n}{r_{ij}^5}\left(1 - \left(\frac{\lambda^3 r_{ij}^3}{6} + \frac{\lambda^2 r_{ij}^2}{2} + \lambda r_{ij} + 1\right)e^{-\lambda r_{ij}}\right) \tag{5}$$

From eq 2, one can construct block matrices 6 and solve eq 7

dx.doi.org/10.1021/ct400549q | J. Chem. Theory Comput. 2013, 9, 5421−5429

Table 2. Parameters for PHASTq, PHAST, and TraPPE Models[a]

	l_{C-O} (Å)	l_{C-X} (Å)	q_C (e)	ε_C (K)	ε_X (K)	σ_C (Å)	σ_X (Å)	α_C (Å^3)	α_O (Å^3)	Θ_{zz}[b] DÅ
CO_2-PHASTq	1.162	1.178	0.6613	24.014	85.817	3.168	2.734			−4.289
CO_2-PHASTq*	1.162	1.187	0.6613	26.894	70.244	3.180	2.755	1.228	0.739	−4.289
CO_2-PHAST	1.162	1.091	0.7710	8.522	76.767	3.055	2.945			−5.003
CO_2-PHAST*	1.162	1.114	0.7714	19.618	46.475	3.034	2.994	1.228	0.739	−5.003
TraPPE[11]	1.16		0.7	27.0	79.0	2.8	3.05			−4.532

[a]X denotes the Lennard-Jones sites along the bond vector. There are two equal negative charges, q_O, on each oxygen center so that the net charge of the molecule is zero. [b]Quadrupole from Chetty et al. −4.29 DÅ.[38]

$$\hat{\mathbf{A}} \equiv \begin{pmatrix} \left[\frac{I}{\alpha_0}\right] & [T_{0,1}] & \cdots & [T_{0,N-1}] \\ [T_{1,0}] & \left[\frac{I}{\alpha_1}\right] & \cdots & [T_{1,N-1}] \\ \cdots & \cdots & \cdots & \cdots \\ [T_{N-1,0}] & [T_{N-1,1}] & \cdots & \left[\frac{I}{\alpha_{N-1}}\right] \end{pmatrix} \tag{6}$$

$$\hat{\mathbf{A}}\vec{\mu} = \vec{\mathrm{E}} \tag{7}$$

which has solutions by either matrix inversion or iterative methods; the latter was the method employed herein. Long-range corrections were handled using an implementation of the Wolf field method,[42−44] which we have recently shown to be efficient and effective. The polarizability model has the advantage that it can include polarizable sites from any other species that is similarly parametrized without further assumptions, thus keeping the entire potential energy in a transferable form. The ostensible disadvantage is the cost of evaluating the many-body function. However, this can be largely offset by iterating efficiently and porting these operations to GPUs.

C. Intermolecular Potential Energy Function. In our PHAST (Potentials with High Accuracy Speed and Transferability) models, CO_2-PHAST and CO_2-PHAST*, where * denotes the inclusion of explicit polarization, the total nonbonded potential energy, U, has contributions from electrostatic interactions, U_{es}, repulsion and dispersion interactions, U_{rd}, and polarization interactions, U_{pol}.

$$U = U_{es} + U_{rd} + U_{pol} \tag{8}$$

The polarization contribution, U_{pol}, of the carbon dioxide model was developed according to the Thole−Applequist polarizability model as explained above. A trial polarizability tensor was created according to the Thole model with exponential damping[41] from scalar point polarizabilities at the atomic coordinates and with the molecule aligned along the Z axis. This trial polarizability tensor was compared with the scaled *ab initio* tensor. The scalar point polarizabilities were varied until the difference between the two tensors was minimized, and the final values are listed in Table 2.

After the point polarizabilities were determined, the parameters of U_{es} and U_{rd} were fit simultaneously via simulated annealing to give a minimum $(U - U_{BO})$, where U_{BO} is the *ab initio* Born−Oppenheimer surface. Similarly to Steinebrunner and Vogel,[19,21] a five-site model was employed to describe the carbon dioxide molecule. The point charges are fixed on the atomic sites, while in a departure from most previous studies, the Lennard-Jones sites are allowed to vary along the bond vector, along with magnitudes for a best fit; this modification is critical in producing a simple potential that captures the correct anisotropy.[29] Four models were parametrized for this investigation. The PHASTq models were fit to the *ab initio* data points with energy below 2500 K and have fixed atomic partial charges that reproduce the quadrupole of −4.287 DÅ. The PHAST models were fit to data points with energy below 5000 K and parametrized by allowing the atomic partial charges to fluctuate as well; allowing the charges to not reproduce the first nonvanishing electric moment results in a better potential energy function. While other models of this type that we have explored reproduced the quadrupole when the charges were allowed to vary,[26,35] this was not the case for the best fit parameters for CO_2. The origin of this effect is not obvious but may be the result of the limitations of the potential form or the nature of the interactions at intermediate distances, where, for example, dispersion may not have yet achieved its asymptotic inverse sixth form.

This result suggests that including other physically motivated terms such as other inverse distance powers (presumably between $1/r$ and $1/r^6$ and not higher order inverse powers characteristic of the asymptotic dispersion expansion) might capture the correct functional form of the interactions and would result in the fits giving the true quadrupole as was found in H_2 and N_2.[26,35] Currently, the parameters for the attractive van der Waals and point electrostatics have to compensate to "best fit" the intermediate behavior, resulting in a more accurate potential but incorrect asymptotic behavior. The compact transferable form that was chosen is a compromise to keep the potential simple and suitable for heterogeneous simulation. Making minimal changes of this type that have strong physical motivations that suggest methods of transferability is the subject of ongoing investigation.

These four models and, for comparison, the TraPPE[11] model parameters are given in Table 2. The TraPPE model is given because it is a highly effective bulk potential fit to reproduce phase coexistence that has been extensively and successfully employed. It will also be shown below that although it is not fit to any *ab initio* data, it nearly exactly reproduces the dimer curves that are well represented in liquid configurations and misrepresents others not important for bulk structure. Note that the TraPPE potential also has a quadrupole larger than the experimental value.

For model validation, Monte Carlo simulations, with the isothermal−isobaric ensemble, of CO_2 at various temperatures and pressures were performed with the software Massively Parallel Monte Carlo (MPMC).[29] For pure CO_2 simulations, the isothermal−isobaric ensemble was used. System sizes ranged from 100 to 150 CO_2 molecules and include averages from 700 000 correlation times, with an additional 700 000 correlation times for state points near a vapor−liquid transition. Simulations of CO_2 adsorption in MOFs were performed via

grand canonical Monte Carlo (GCMC). The probability of molecule insertion/deletion was set to 0.3.[3] The chemical potential of CO_2 was mapped to the pressure by the Peng–Robinson equation of state.[45] Three MOFs were chosen to simulate CO_2 sorption: Zn_4O(1,4-benzenedicarboxylate)$_3$ (MOF-5),[46] [Cu(4,4′-dipyridylacetylene)$_2$$SiF_6$-i] (also known as SIFSIX-2-Cu-i),[47] and [Cu(H_2O)]$_3$(5,5′,5″-benzene-1,3,5-triyltris(1-ethynyl-2-isophthalate)) (PCN-61).[48] All metal–organic frameworks were modeled as rigid frameworks. The MOF-5 potential parameters used in GCMC simulations were that of Belof et al.[49] PCN-61 and [Cu(dpa)$_2$$SiF_6$-i] were established according to previous work.[43,44] Simulations with MOF-5 were run for 300 000 correlation times, and simulations with [Cu(dpa)$_2$$SiF_6$-i][44] and PCN-61[43] were run for 10^6 correlation times.

III. RESULTS AND DISCUSSION

A. *Ab Initio* Results. Figure 1 gives the *ab initio* interaction energy curves for five carbon dioxide dimers. The largest interaction energy is from the slipped parallel (S) configuration, which is 5% larger than that reported by previous authors at similar dimer separation distances.[18,20,21] The interaction energy of the T configuration is 3% larger than previous reports, while the separation distance is consistent with such reports.

Figure 1 also shows the intermolecular potential models compared with the *ab initio* curves. Note that only the models without explicit polarization are plotted. The CO_2-PHASTq* and CO_2-PHAST* curves are excluded because they lie on top of the CO_2-PHASTq and CO_2-PHAST results, respectively. All PHAST and PHASTq models have better fits to the repulsive region of all *ab initio* curves compared with the TraPPE model. The TraPPE model fits the attractive region of the X, P, and S dimer interaction curves well. This trend is expected since the TraPPE parameters were fitted from vapor–liquid equilibria data, and liquids inherently minimize repulsive configurations. Furthermore, the PHASTq and PHAST models fit closer to the *ab initio* curve for the E configuration, which is unsurprising since the E configuration is highly repulsive and would have a low occurrence in the liquid state. Because of the simplicity of the functional form and the anisotropy of the potential energy surface, neither the TraPPE, PHASTq, nor PHAST models predict the S configuration to be the minimum energy dimer structure.

Comparing the PHAST and PHASTq models, the PHASTq models fit better to the *ab initio* curves for configurations E, T, and X, but worse for the P configuration. Conversely, the PHAST models underestimate the minimum energy for the X configuration. These differences can be attributed to the larger partial charges of the PHAST models compared with the PHASTq models.

B. Model Validation. *1. Pressure–Density Isotherms.* Each model was used in NPT Monte Carlo simulations of CO_2 at various temperatures and pressures and compared with experimental data from IUPAC.[50] Figures 2, 3, and 4 give the pressure–density isotherms at the temperatures 298.15, 350.15, and 500.15 K, respectively. At 298.15 K (Figure 2), the TraPPE model produces the correct density for all pressures from 0.5 to 500 atm. The two PHASTq models give a density 10% larger in the liquid region. The CO_2-PHAST* model correctly produces gas phase densities from 0.5 to 40 atm and liquid phase densities from 300 to 500 atm. Radial distribution function plots were created for three state points below the critical

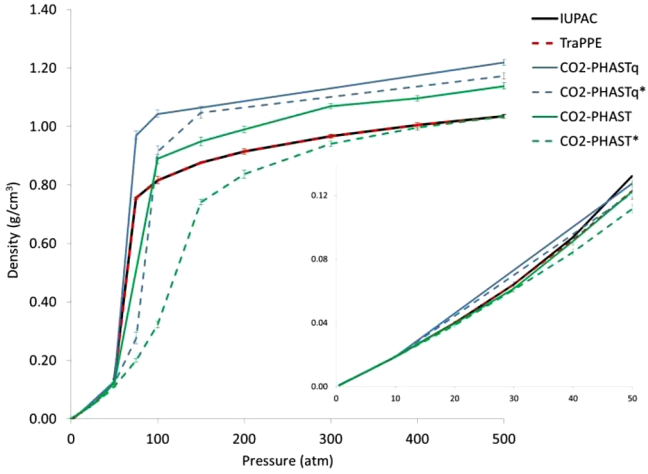

Figure 2. Pressure–density plot of carbon dioxide at 298.15 K. Inset graph is from 0 to 50 atm.

temperature in order to compare the fluid structures, and they are shown in Figure 5.

Above the critical point, at 350.15 K (Figure 3), all models do well from 0.5 to 75 atm. The CO_2-PHAST* model

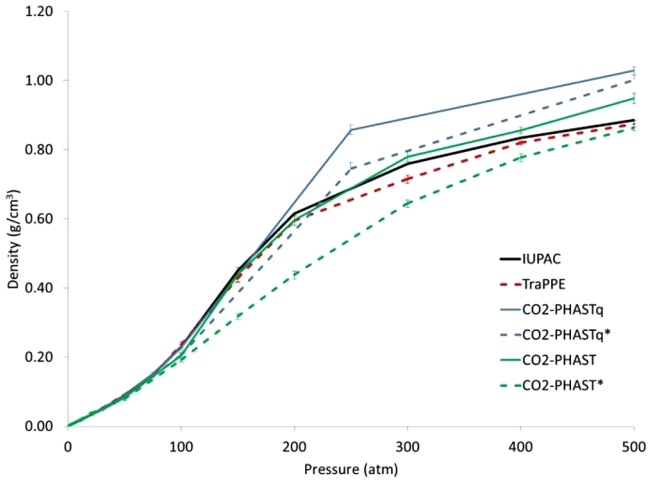

Figure 3. Pressure–density plot of carbon dioxide at 350.15 K.

underestimates the densities in the pressure range 100 to 400 atm, while the CO_2-PHASTq models overestimate the density from 200 to 500 atm. As with the 298.15 K isotherms, the TraPPE model produces an isotherm that is in excellent agreement with experiment at 350.15 K for the pressure range considered.

At 500 K (Figure 4), the CO_2-PHAST and CO_2-PHAST* models reproduce the experimental densities reasonably well from 0.5 to 500 atm. The CO_2-PHAST* model underestimates the density by 8% in the range of 300–500 atm. Note that the TraPPE model is accurate in this region as well.

Note that the CO_2-PHASTq and CO_2-PHASTq* models have similar charges, epsilons, and sigmas as the TraPPE model but the CO_2-PHAST and CO_2-PHAST* do not. This parameter set represents a different compromise between the limited function form allowed in the compact description of CO_2 interactions. To investigate the structural origins of the differing densities plotted in Figure 2, the radial distribution function, g(r), was plotted for three state points and is shown in

dx.doi.org/10.1021/ct400549q | J. Chem. Theory Comput. 2013, 9, 5421–5429

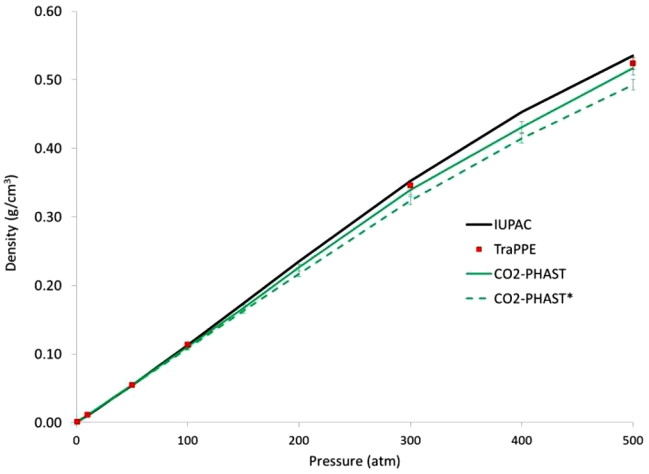

Figure 4. Pressure−density plot of carbon dioxide at 500.15 K.

Figure 5. The fluid structures of the PHAST and PHASTq models are quite similar to that of the TraPPE model at pressures of 10 and 500 atm at 298 K. The CO_2-PHAST* model shows a less structured fluid than the others at 298 K and 100 atm (Figure 5b). All models agree with the recent publication by Neuefeind et al. that gives a C−C pair distribution function maximum at 3.95 Å for liquid CO_2 at 298 K and 66 bar.[51] Thus, it appears that a large number of potentials of this form can reproduce bulk structure and thermodynamics, making the choice of potential parameters underdetermined. More work is needed to establish better compact transferable forms where this uncertainty may be resolved.

The energetics of solid CO_2 were examined using the PHAST and PHASTq models, and the minimum energy structure gave lattice parameters of 5.32 to 5.34 Å for the *Pa*3 face-centered cubic crystal. Literature values for the lattice parameter for the same thermal crystal range from 5.624 to 5.494 Å.[52,53] The proposed potentials are reasonable bulk models albeit not as effective as, for example, TraPPE; however, this appears to be the compromise in order to produce a potential that can better function in heterogeneous environments as will be demonstrated next.

2. Simulations in MOFs. Monte Carlo simulations with the μVT ensemble were performed with the PHAST, PHASTq, and TraPPE potentials. Figure 6 shows the absolute CO_2 uptake in MOF-5 at 298.15 K. The isotherms from simulation were corrected for the latest Brunauer−Emmett−Teller (BET) surface area calculation of 3800 m^2/g.[54] Specifically, the original isotherms were scaled by the factor 2833/3800, as the crystal structure of MOF-5 used in this work has a surface area of 2833 m^2/g as reported by Millward et al.[55] MOF-5 is a network of 1,4-benzenedicarboxylate (BDC) linked to zinc tetramers with very little charge separation on the framework,[49] and it is expected that polarization effects would be negligible for sorption in this MOF. As determined from the simulations, polarization accounts for 6% and 11% of the total energy for the CO_2-PHASTq* and the CO_2-PHAST* models, respectively. Previous GCMC simulations of CO_2 adsorption in MOF-5 by Skoulidas et al.[4] used the EPM2[12] potential for CO_2 and Lennard-Jones parameters from UFF[56] for the MOF-5 framework. Only Lennard-Jones interactions were considered, and the resulting uptakes were higher than experiment. The GCMC simulation of CO_2 sorption in MOF-5 performed by

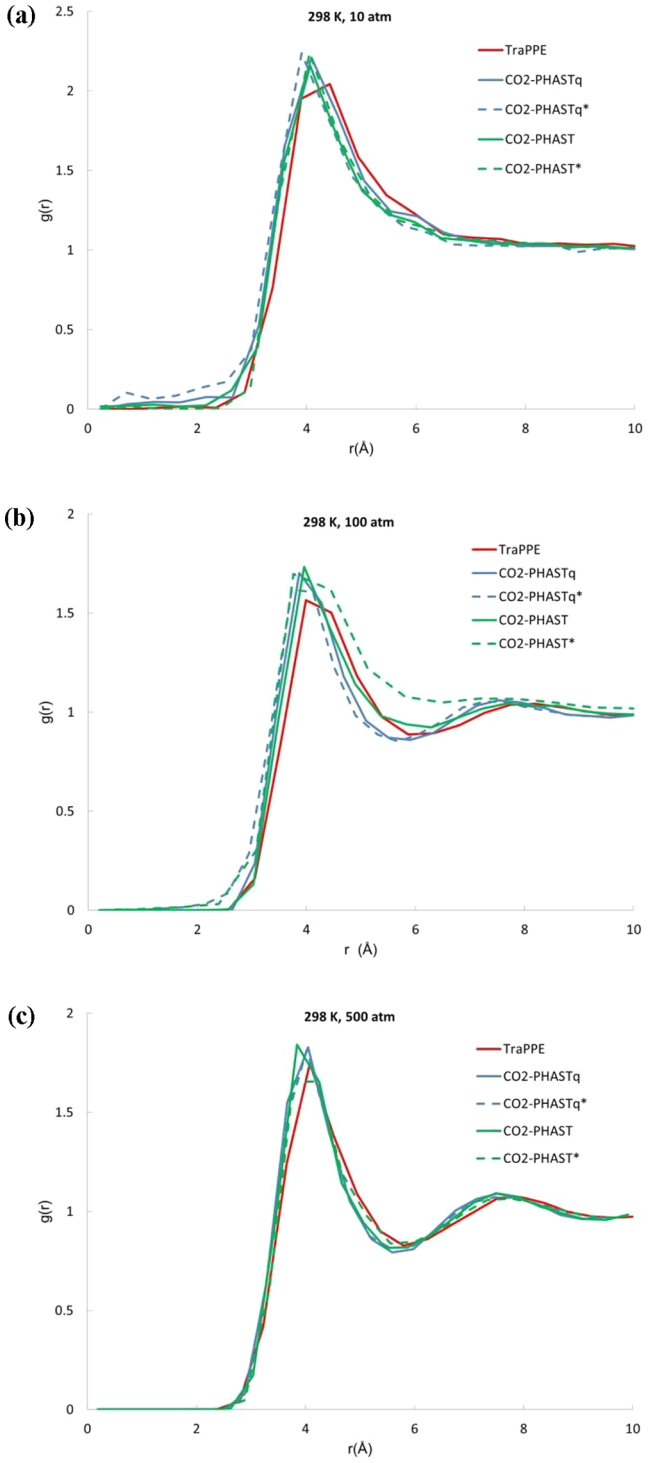

Figure 5. Radial distribution function, g(r), for (a) dense gaseous bulk carbon dioxide at 298.15 K and 10 atm, (b) bulk carbon dioxide at 298.15 K and 100 atm, and (c) liquid bulk carbon dioxide at 298.15 K and 500 atm. The distance is taken from the center-of-mass of each molecule.

Babarao et al. was an improvement, as the framework was assigned atomic partial charges to reproduce the electrostatic potential surface; however the uptakes are also higher than experiment.[57] The PHASTq models have comparable Lennard-Jones values to the TraPPE and EPM2 models and produced higher uptakes as well. The PHAST models have reduced epsilon values and predict uptakes that are in best agreement

dx.doi.org/10.1021/ct400549q | J. Chem. Theory Comput. 2013, 9, 5421−5429

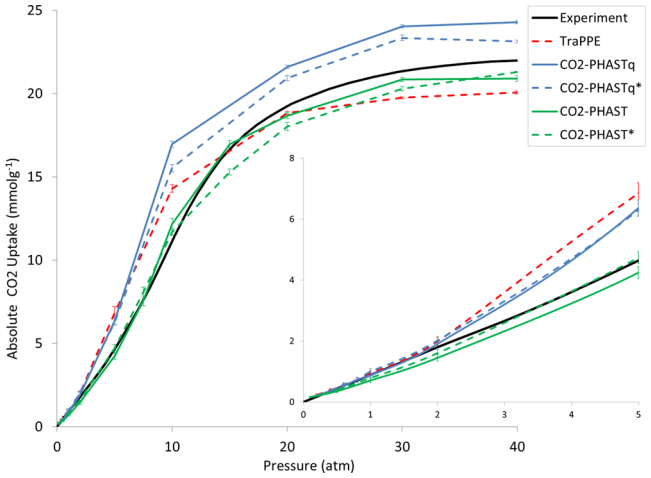

Figure 6. CO_2 sorption isotherms in MOF-5 at 298.15 K. Inset graph is from 0 to 5 atm.

with experiment. The TraPPE model is an adequate potential as expected and underestimates the maximum loading by only 8%; however, it does not do well for modeling low pressure CO_2 uptake.

The [Cu(dpa)$_2$SiF$_6$-i] square-pillared metal−organic material (MOM) is water stable and shows promise for applications in CO_2 sorption and separation.[47] This structure is highly polar with SiF_6^{2-} moieties, but recent theoretical studies on this compound demonstrate that polarization effects are negligible due to the narrow pore size.[44] Indeed, sorption in [Cu(dpa)$_2$SiF$_6$-i] is dominated by van der Waals interactions. All CO_2 models (TraPPE, PHASTq, and PHAST) were tested in this MOM and compared with experimental results. It can be observed that the PHAST models produce isotherms that are in very good agreement with the experimental data (Figure 7).

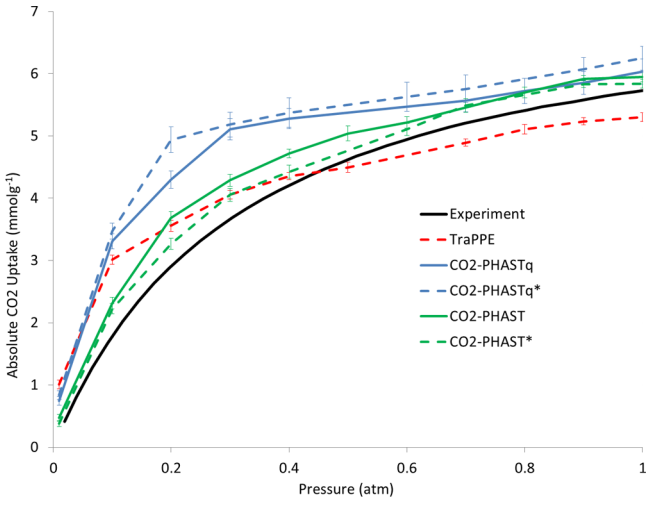

Figure 7. CO_2 sorption isotherms in [Cu(dpa)$_2$SiF$_6$-i] at 298 K and pressures up to 1.0 atm.

The CO_2-PHAST* model provides the best agreement with experiment while the CO_2-PHAST model produces slightly higher uptakes. This is because polarization causes a favorable sorbate ordering of CO_2 molecules in the MOM, which decreases overall sorption. In general, the PHASTq models produce higher uptakes than the PHAST models in the compound; this can be attributed to the greater potential well depth of the T configuration associated with the PHAST models. Note that polarization accounts for 9−10% in both polar PHAST/PHASTq models. Similarly to the isotherms for MOF-5, the TraPPE model overestimates the experimental isotherm at low pressure CO_2 sorption and underestimates at higher pressures.

Simulation of CO_2 sorption was performed using the TraPPE, PHASTq, and PHAST models in PCN-61. This is a prototypical polar *rht*-MOF that was chosen for baseline computational studies. Previous work involving H_2 sorption in PCN-61 showed that many-body polarization interactions were essential to capture the correct sorption behavior in the MOF.[43] GCMC simulations of CO_2 sorption were performed using the PCN-61 force field that was developed by Forrest et al. Figure 8a shows the low-pressure excess sorption isotherms

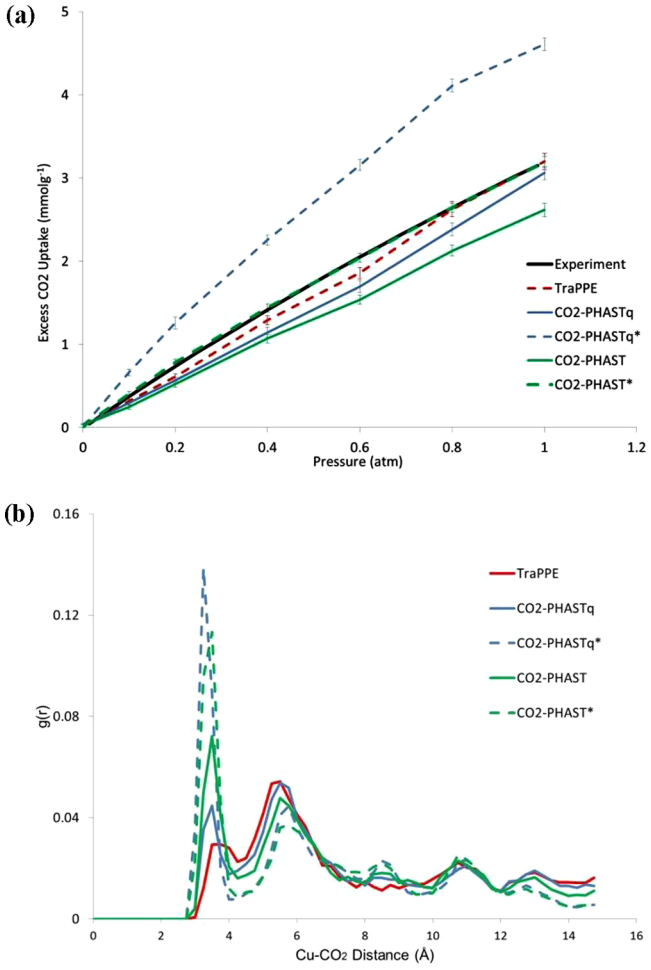

Figure 8. (a) CO_2 sorption isotherms in PCN-61 at 298 K and pressures up to 1.0 atm and (b) radial distribution function, $g(r)$, about the exterior Cu ion in PCN-61 at 298 K and 0.20 atm.

at 298 K for the five models compared with experimental data. It can be seen that the CO_2-PHAST model undersorbs the experimental data across all loadings, while the CO_2-PHAST* model produced an isotherm that is in excellent agreement with the experiment.[58] The difference between the CO_2-PHAST and CO_2-PHAST* isotherms in PCN-61 demonstrate the importance of explicit polarization for the modeling of gas sorption in a polar MOF with high surface area and open-metal sites. The isotherm generated by the CO_2-PHASTq model is

dx.doi.org/10.1021/ct400549q | J. Chem. Theory Comput. 2013, 9, 5421−5429

higher than that of the CO_2-PHAST models, which is a direct consequence of the larger epsilon parameters for the former. It is important to note that the CO_2-PHASTq* model produces an isotherm that is much higher than experiment across all loadings in PCN-61, despite having the correct quadrupole, the inclusion of polarization, and slightly smaller epsilon values than the TraPPE model. From this, it can be deduced that simulations using the CO_2-PHASTq* model in PCN-61 result in sorption to regions that are dominated by van der Waals and electrostatic interactions as well as induction simultaneously. In contrast, van der Waals interactions contribute much less to the sorption structure for the CO_2-PHAST model. At 1.0 atm, polarization accounts for 15.9% (CO_2-PHASTq*) and 16.7% (CO_2-PHAST*) of the total energy. The TraPPE model slightly undersorbs the experimental isotherm at initial loading but comes into agreement at pressures approaching 1.0 atm.

Although the TraPPE model can be seen agreeing well with the experimental isotherm with respect to raw uptake, it inadequately captures the most prominent MOF−sorbate interaction. Figure 8b shows the radial distribution functions of CO_2 molecules about the exterior Cu^{2+} ions (the ions projecting into the cuboctahedral cage of the MOF) for all five models at low loading. The radial distribution functions are normalized to a total magnitude of unity over the distance examined. This was chosen to obtain a direct comparison between the relative magnitudes for each model. The CO_2-PHASTq* and CO_2-PHAST* models produced a large peak at ca. 3.25 Å, which corresponds to a significant population of CO_2 molecules sorbing onto the open-metal site. Note that this peak is consistent with the observed CO_2−Cu distance in HKUST-1, a prototypical MOF containing 1,3,5-benzenetricarboxylate linkers coordinated to Cu^{2+} ions, as determined from neutron powder diffraction and *ab initio* studies.[59] A reasonable peak can also be seen for the CO_2-PHAST model at that distance, although the magnitude is approximately half that of the CO_2-PHAST* model. The CO_2-PHASTq model produces a smaller peak at 3.25 Å than the CO_2-PHAST model, which can be explained by the smaller partial charges for the former. Thus, while the isotherm for the CO_2-PHASTq model is higher than that for the CO_2-PHAST model in PCN-61, the radial distribution functions demonstrate that the occupancy about the metal centers for the CO_2-PHASTq model is not comparable to those for the CO_2-PHAST model. The TraPPE model produced the smallest peak of the five models at 3.25 Å, which signifies that there is little occupation of CO_2 molecules about the open-metal site. These results demonstrate that although the CO_2-PHAST* and TraPPE model produced similar uptakes in PCN-61, only the polarizable model captures the critical interaction between the CO_2 molecules and the open-metal sites. Note, however, that the nonpolar PHAST/PHASTq models give a far more reasonable structure than the TraPPE model, which does not capture the sorbate−metal interaction peak. The majority of TraPPE CO_2 molecules can be seen sorbing into regions that are dominated by van der Waals and electrostatic interactions in PCN-61, such as the corners of the truncated tetrahedral cages (see below). Other than the difference in magnitudes of the 3.25 Å radial distribution peak, the distribution of CO_2 molecules among all five models are similar with increasing distance from the metal ion. It is important to note that the CO_2−Cu interaction in PCN-61 is characterized as physisorption, not chemisorption. Evaluation of the binding energy for a CO_2 molecule sorbed onto the Cu^{2+} ion via calculation of the isosteric heat of adsorption, Q_{st}, in experiment and simulation revealed that the adsorption energy ranges from 20 to 30 kJ/mol. Although the CO_2 molecule sorbs onto the open-metal sites using the PHAST/PHASTq models, the inclusion of explicit polarization results in a much stronger CO_2−Cu interaction, and thus, a larger nearest-neighbor peak is seen for the CO_2-PHAST* and CO_2-PHASTq* models.

Figure 9 shows the 3D histograms revealing the most frequent sites of CO_2 occupancy in PCN-61 at low loading for

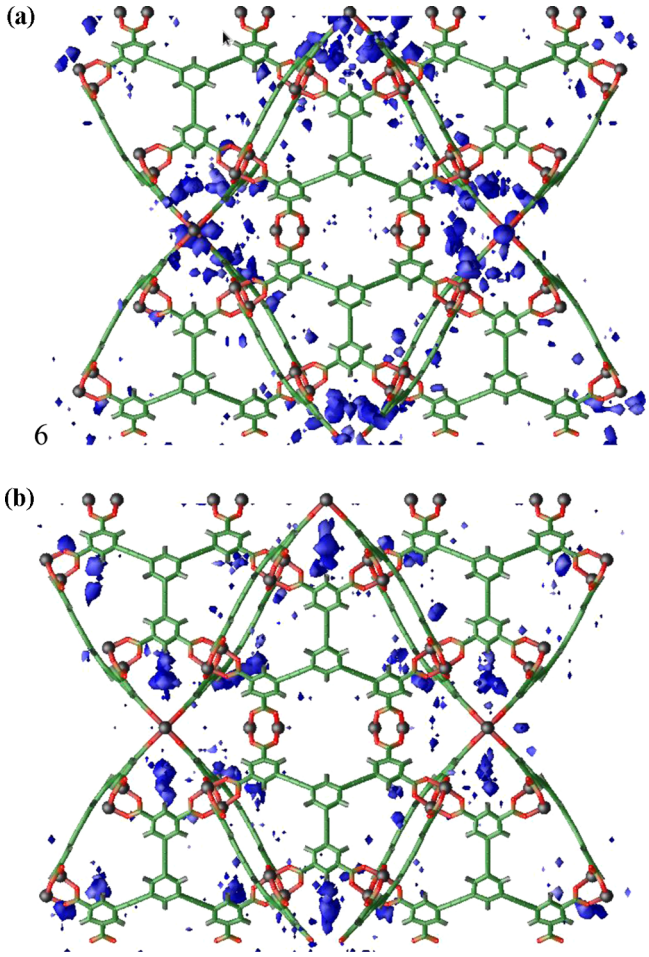

Figure 9. Three-dimensional histogram showing the most frequent sites of CO_2 occupancy (blue) in PCN-61 at low loading using (a) the CO_2-PHAST* model and (b) the TraPPE model.

both the CO_2-PHAST* and TraPPE models, respectively. For the polarizable model, there is significant sorption onto the exterior Cu^{2+} ions of the copper paddlewheels at low loading. Thus, as expected, sorption onto the open-metal sites is captured using this potential. In contrast, for the TraPPE model, the CO_2 molecules mostly coordinate to the corners of the truncated tetrahedral cage at initial loading. This region is dominated by van der Waals and electrostatic interactions, which is where the majority of CO_2 molecules sorb using the TraPPE model. Note that significant sorption onto metals is not seen for the TraPPE model.

IV. CONCLUSION

Here, we introduced the PHAST potentials that are a compromise between exactly reproducing the *ab initio* dimer curves for carbon dioxide and having a limited, compact

dx.doi.org/10.1021/ct400549q | J. Chem. Theory Comput. 2013, 9, 5421−5429

description. The PHAST models were compared with the excellent bulk TraPPE potential. Interestingly, the TraPPE CO_2 model was shown to reproduce the *ab initio* dimer curves for configurations occurring most often in the liquid state (even though not fit to them) but is less effective in capturing configurations not frequently occurring in the bulk.

The proposed PHAST models perform well for all geometries (including those that are absent in bulk fluids, yet important in sorption) and includes polarization, which makes the potential suitable for simulations with induced-dipole interactions. The resulting potentials have been shown to be reasonably effective for bulk simulations and very efficient for modeling CO_2 at charged/polar interfaces. The PHAST models, compared with PHASTq models, have larger partial charges and reduced Lennard-Jones well depths, shifting the energy composition to more electrostatic in nature, with less emphasis on van der Waals interactions. This shift accounts for the improved initial CO_2 uptake in MOFs, since it directs the CO_2 molecules to metal centers first. The PHAST models are recommended for materials simulation.

For the three MOFs in which simulations of CO_2 sorption were investigated herein, the CO_2-PHAST* model provided the best agreement with experimental data. The maximum calculated errors for the CO_2-PHAST* model in MOF-5, $[Cu(dpa)_2SiF_6\text{-i}]$, and PCN-61 are ±0.33, ±0.11, and ±0.07 mmol/g, respectively. The CO_2-PHAST model produced an isotherm that is in good agreement with experiment in MOF-5 and $[Cu(dpa)_2SiF_6\text{-i}]$; however, the lack of explicit polarization causes this model to undersorb the experimental isotherm in PCN-61. The CO_2-PHASTq model oversorbs in MOF-5 and $[Cu(dpa)_2SiF_6\text{-i}]$ but undersorbs slightly in PCN-61. The isotherms generated by the CO_2-PHASTq* model significantly oversorbed the experimental results for all three MOFs. For simulations using the TraPPE model in MOF-5 and $[Cu(dpa)_2SiF_6\text{-i}]$, the generated isotherm oversorbed experiment at low pressures and then undersorbed at higher pressures. Further, although the TraPPE model produces an isotherm that is in good agreement with experiment in PCN-61, it is clear from Figure 8b that the TraPPE CO_2 molecules are farther away from the Cu^{2+} ions, which is in contrast to the experimentally observed CO_2–Cu^{2+} interaction. It is next planned to use the PHAST models for simulations of CO_2 sorption in other MOFs.

AUTHOR INFORMATION

Corresponding Author

*E-mail: brian.b.space@gmail.com.

Notes

The authors declare no competing financial interest.

ACKNOWLEDGMENTS

This work was supported by the National Science Foundation (Award No. CHE-1152362). Computations were performed under an XSEDE Grant (No. TG-DMR090028) to B.S. This publication is also based on work supported by Award No. FIC/2010/06, made by King Abdullah University of Science and Technology (KAUST). The authors also thank the Space Foundation (Basic and Applied Research) for partial support. The authors acknowledge the use of the services provided by Research Computing at the University of South Florida.

REFERENCES

(1) Yang, H.; Xu, Z.; Fan, M.; Gupta, R.; Slimane, R. B.; Bland, A. E.; Wright, I. *J. Environ. Sci.* **2008**, *20*, 14–27.
(2) Li, J.-R.; Ma, Y.; McCarthy, M. C.; Sculley, J.; Yu, J.; Jeong, H.-K.; Balbuena, P. B.; Zhou, H.-C. *Coord. Chem. Rev.* **2011**, *255*, 1791–1823.
(3) Garberoglio, G.; Skoulidas, A. I.; Johnson, J. K. *J. Phys. Chem. B* **2005**, *109*, 13094–13103.
(4) Skoulidas, A. I.; Sholl, D. S. *J. Phys. Chem. B* **2005**, *109*, 15760–15768.
(5) Liu, J.; Keskin, S.; Sholl, D. S.; Johnson, J. K. *J. Phys. Chem. C* **2011**, *115*, 12560–12566.
(6) Ehlig-Economides, C.; Economides, M. J. *J. Pet. Sci. Eng.* **2010**, *70*, 123–130.
(7) Kobashi, K.; Kihara, T. *J. Chem. Phys.* **1980**, *72*, 3216–3220.
(8) Murthy, C. S.; Singer, K.; McDonald, I. R. *Mol. Phys.* **1981**, *44*, 135–143.
(9) Etters, R. D.; Kuchta, B. *J. Chem. Phys.* **1989**, *90*, 4537–4541.
(10) Moller, D.; Fischer, J. *Fluid Phase Equilib.* **1994**, *100*, 35–61.
(11) Potoff, J. J.; Siepmann, J. I. *AIChE J.* **2001**, *47*, 1676–1682.
(12) Harris, J. G.; Yung, K. H. *J. Phys. Chem.* **1995**, *99*, 12021–12024.
(13) Zhang, Z. G.; Duan, Z. H. *J. Chem. Phys.* **2005**, *122*, 214507.
(14) Zhang, Y.; Yang, J.; Yu, Y.-X. *J. Phys. Chem. B* **2005**, *109*, 13375–13382.
(15) Merker, T.; Engin, C.; Vrabec, J.; Hasse, H. *J. Chem. Phys.* **2010**, *132*, 234512.
(16) Welker, M.; Steinebrunner, G.; Solca, J.; Huber, H. *Chem. Phys.* **1996**, *213*, 253–261.
(17) Tsuzuki, S.; Uchimaru, T.; Tanabe, K.; Kuwajima, S.; Tajima, N.; Hirano, T. *J. Phys. Chem.* **1996**, *100*, 4400–4407.
(18) Tsuzuki, S.; Uchimaru, T.; Mikami, M.; Tanabe, K. *J. Chem. Phys.* **1998**, *109*, 2169–2175.
(19) Steinebrunner, G.; Dyson, A. J.; Kirchner, B.; Huber, H. *J. Chem. Phys.* **1998**, *109*, 3153–3160.
(20) Bukowski, R.; Sadlej, J.; Jeziorski, B.; Jankowski, P.; Szalewicz, K.; Kucharski, S. A.; Williams, H. L.; Rice, B. M. *J. Chem. Phys.* **1999**, *110*, 3785–3802.
(21) Bock, S.; Bich, E.; Vogel, E. *Chem. Phys.* **2000**, *257*, 147–156.
(22) Yu, K.; McDaniel, J. G.; Schmidt, J. R. *J. Phys. Chem. B* **2011**, *115*, 10054–10063.
(23) Bohm, H. J.; Meissner, C.; Ahlrichs, R. *Mol. Phys.* **1984**, *53*, 651–672.
(24) Yang, J.; Ren, Y.; Tian, A.-m. *J. Phys. Chem. B* **2000**, *104*, 4951–4957.
(25) Werner, H. J.; Knowles, P. J.; Knizia, G.; Manby, F. R.; Schutz, M.; et al. *Molpro, version 2010.0, a package of ab initio programs*, 2010.
(26) McLaughlin, K.; Cioce, C. R.; Belof, J. L.; Space, B. *J. Chem. Phys.* **2012**, *136*, No. 194302.
(27) Huber, K. P.; Herzberg, G., *Molecular Spectra and Molecular Structure IV. Constants of Diatomic Molecules*; Van Nostrand Reinhold Co.: New York, 1979.
(28) Mankoo, P. K.; Keyes, T. *J. Chem. Phys.* **2008**, *129*, No. 034504.
(29) Belof, J. L.; Stern, A. C.; Space, B. *J. Chem. Theory Comput.* **2008**, *4*, 1332–1337.
(30) Raghavachari, K.; Trucks, G. W.; Pople, J. A.; Head-Gordon, M. *Chem. Phys. Lett.* **1989**, *157*, 479–483.
(31) Dunning, T. H., Jr. *J. Chem. Phys.* **1989**, *90*, 1007–1023.
(32) Kendall, R. A.; Dunning, T. H. J. *J. Chem. Phys.* **1992**, *96*, 6796–6806.
(33) Huh, S. B.; Lee, J. S. *J. Chem. Phys.* **2003**, *118*, 3035–3042.
(34) Boys, S. F.; Bernardi, F. *Mol. Phys.* **1970**, *19*, 553–566.
(35) Cioce, C. R.; McLaughlin, K.; Belof, J. L.; Space, B. *J. Chem. Theory Comput.* **2013**, DOI: 10.1021/ct400526a.
(36) Graham, C.; Imrie, D. A.; Raab, R. E. *Mol. Phys.* **1998**, *93*, 49–56.
(37) Coriani, S.; Halkier, A.; Rizzo, A.; Ruud, K. *Chem. Phys. Lett.* **2000**, *326*, 269–276.
(38) Chetty, N.; Couling, V. W. *Mol. Phys.* **2011**, *109*, 655–666.
(39) Karna, S.; Dupuis, M. *J. Comput. Chem.* **1991**, *12*, 487.

(40) Applequist, J.; Carl, J. R.; Fung, K.-K. *J. Am. Chem. Soc.* **1972**, *94*, 2952−2960.
(41) van Duijnen, P. T.; Swart, M. *J. Phys. Chem. A* **1998**, *102*, 2399−2407.
(42) Wolf, D.; Keblinski, P.; Phillpot, S. R.; Eggebrecht, J. *J. Chem. Phys.* **1999**, *110*, 8254−8282.
(43) Forrest, K. A.; Pham, T.; McLaughlin, K.; Belof, J. L.; Stern, A. C.; Zaworotko, M. J.; Space, B. *J. Phys. Chem. C* **2012**, *116*, 15538−15549.
(44) Pham, T.; Forrest, K. A.; McLaughlin, K.; Tudor, B.; Nugent, P.; Hogan, A.; Mullen, A.; Cioce, C. R.; Zaworotko, M. J.; Space, B. *J. Phys. Chem. C* **2013**, *117*, 9970−9982.
(45) Poling, B. E.; Prausnitz, J. M.; O'Connell, J. P. *The Properties of Gases and Liquids*, 5th ed.; McGraw-Hill Professional: New York, 2000.
(46) Li, H.; Eddaoudi, M.; O'Keefe, M.; Yaghi, O. M. *Nature* **1999**, *402*, 276−279.
(47) Nugent, P.; Belmabkhout, Y.; Burd, S. D.; Cairns, A. J.; Luebke, R.; Forrest, K.; Pham, T.; Ma, S.; Space, B.; Wojtas, L.; Eddaoudi, M.; Zaworotko, M. J. *Nature* **2013**, *495*, 80−84.
(48) Zhao, D.; Yuan, D.; Sun, D.; Zhou, H.-C. *J. Am. Chem. Soc.* **2009**, *131*, 9186−9188.
(49) Belof, J. L.; Stern, A. C.; Space, B. *J. Phys. Chem. C* **2009**, *113*, 9316−9320.
(50) Angus, S.; Armstrong, B.; Reuck, K. M. d., *Carbon Dioxide International Thermodynamic Tables of the Fluid State- 3*, 1st ed.; Pergamon Press Inc.: Elmsford, NY, 1976.
(51) Neuefeind, J.; Fischer, H. E.; Simonson, J. M.; Idrissi, A.; Schops, A. *J. Chem. Phys.* **2009**, *130*, No. 174503.
(52) Simon, A.; Peters, K. *Acta Crystallogr.* **1980**, *B36*, 2750−2751.
(53) Downs, R. T.; Somayazulu, M. S. *Acta Crystallogr.* **1998**, *C54*, 897−898.
(54) Kaye, S. S.; Dailly, A.; Yaghi, O. M.; Long, J. R. *J. Am. Chem. Soc.* **2007**, *129*, 14176−14177.
(55) Millward, A. R.; Yaghi, O. M. *J. Am. Chem. Soc.* **2005**, *127*, 17998−17999.
(56) Rappe, A. K.; Casewit, C. J.; Colwell, K. S.; Goddard, W. A. I.; Skiff, W. M. *J. Am. Chem. Soc.* **1992**, *114*, 10024−10035.
(57) Babarao, R.; Hu, Z.; Jiang, J. *Langmuir* **2007**, *23*, 659−666.
(58) Zheng, B.; Bai, J.; Wojtas, L.; Zaworotko, M. J. *J. Am. Chem. Soc.* **2011**, *133*, 748−751.
(59) Wu, H.; Simmons, J. M.; Srinivas, G.; Zhou, W.; Yildirim, T. *J. Phys. Chem. Lett.* **2010**, *1*, 1946−1951.